International Journal of Nanomedicine

Dovepress
open access to scientific and medical research

Open Access Full Text Article

ORIGINAL RESEARCH

Multifunctional Quaternary Phosphorus/Bromoargentate Hybrids: The Achievement of Greenish Blue Luminescence, Repeatable Photocurrent Responses and Durable Antimicrobial Activities with Enhanced Water Stability

This article was published in the following Dove Press journal:
International Journal of Nanomedicine

Jing-Bo Liu[1]
Qiao-Jun Zhang[2]
Jian-Zhi Liu[1]
Wen-Ting Zhang[3]
Yi Li[3]
Hao-Hong Li[3]
Zhi-Rong Chen[3]
Da-Li Zheng[2]

[1]Department of Otorhinolaryngology, Fujian Medical University Union Hospital, Fuzhou, Fujian 350001, People's Republic of China; [2]Fujian Key Laboratory of Oral Diseases, Fujian Biological Materials Engineering and Technology Center of Stomatology, School and Hospital of Stomatology, Fujian Medical University, Fuzhou, Fujian 350004, People's Republic of China; [3]College of Chemistry, Fuzhou University, Fuzhou, Fujian 350116, People's Republic of China

Correspondence: Da-Li Zheng
Fujian Key Laboratory of Oral Diseases, Fujian Biological Materials Engineering and Technology Center of Stomatology, School and Hospital of Stomatology, Fujian Medical University, 88 Jiaotong Road, Fuzhou 350004, People's Republic of China
Tel +86-591-83720599
Email dalizheng@fjmu.edu.cn

Jian-Zhi Liu
Department of Otorhinolaryngology, Fujian Medical University Union Hospital, 29 Xinquan Road, Fuzhou 350001, People's Republic of China
Tel +86-591- 83357896
Email liujianzhi@aliyun.com

Background: The realization of multifunction in one bulk material is fascinating for developing a new generation of devices. Quaternary phosphorus salts were seldom utilized as templates in haloargentate systems, and the hybridization of alkyl(triphenyl)phosphonium with halometallate will be a good strategy for the development of multifunctional material, especially for biological material.

Methods: Under the template of (triphenyl)phosphonium-based quaternary phosphorus salts with different spacer lengths (n=2, 3, 4), three bromoargentate hybrids were constructed via the solution method, ie, (1,2-DBTPP)(Ag_2Br_4) (**1**), $\{(1,3\text{-DBTPP})_2(Ag_7Br_{11})]\cdot CH_3CN\cdot H_2O\}_n$ (**2**), and $\{[(1,4\text{-DBTPP})(Ag_5Br_7)](CH_3CN)_2\cdot H_2O\}_n$ (**3**) (1,2-DBTPP^{2+}=ethane-1,2-diylbis (triphenyl)phosphonium, 1,3-DBTPP^{2+}=propane-1,3-diylbis (triphenyl)phosphonium, 1,4-DBTPP^{2+}=butane-1,4-diylbis (triphenyl)phosphonium)).

Results: The $(Ag_7Br_{11})_n^{4n-}$ chain in **2** is a new type of 1-D bromoargentate chain constructed from cubane-like Ag_4Br_4 nodes, $AgBr_4$ tetrahedrons and $AgBr_3$ triangles. Interestingly, by elongating spacer n from 2 to 4, argentophilicity interactions are weakened, and the hydrogen bonds are strengthened. Consequently, their water stabilities and photocurrents are improved, in which the Ag-4d/Br-4p to π* anti-bonding orbital of the quaternary phosphorus transfer is facilitated. Furthermore, the greenish blue emissions can be detected. Finally, high inhabitation rates against *Streptococcus mutans* and *Candida albicans* can be observed in **2** and **3**.

Conclusion: In all experiments, by elongating the spacer lengths of quaternary phosphorus salts, multifunctions were integrated in the quaternary phosphorus/bromoargentate hybrids, including greenish blue luminescence, repeatable photocurrent responses and durable antimicrobial activities with enhanced water stability. This work could provide a theoretical guide for the design of new biologically multifunctional materials.

Keywords: quaternary phosphorus, bromoargentates, nanoparticles, luminescence, antimicrobial

Introduction

In the past decades, halometallate-based functional materials have attracted great attention due to their versatile structure and unique properties, based on which many novel applications have emerged, such as perovskite solar cells,[1,2] luminescence,[3] molecular switches,[4] nonlinear-optic devices[5] and chromisms.[6] Among the

halometallate hybrids, d^{10} silver(I) halides have captured special interest for the following reasons: first, various anion dimensionalities based on rich coordination geometries of the Ag(I) ion (from linear MX_2, triangular MX_3, tetrahedral MX_4, and octahedral AgX_6) and variable connection modes;[7] second, unique physical properties of electron-rich halo-argentates.[8] To date, in the halo-argentate-based hybrids, the templates include organic cations, metal ions and metal-organic complexes.[9,10] In the organic templated haloargentate hybrids, most of them are N/S-bearing organic cations with different ligand spacers and terminal substituent groups and hydrophobicity. For example, the increased number of methyl substituents in the organic templates can result in more inorganic/organic interactions, which is favorable for the formation of complicated haloargentate chains.[11] However, quaternary phosphorus salts were seldom utilized as templates in haloargentate system, and only limited haloargentate/quaternary phosphorus hybrids were reported.[12–14] The hybridization of alkyl(triphenyl)phosphonium with halometallate will be a good strategy for the development of multifunctional material.[15] First, the tetrahedral geometry of alkyl(triphenyl)phosphonium cations limits benzene-benzene π–π stacking interactions in the lattice; consequently, long persistence phosphors might be achieved. Second, in alkyl(triphenyl)phosphonium/halometallate hybrids, the LUMOs were commonly localized on the phosphine ligands, while the HOMOs were occupied by halometallates.[16–18] The cationization of phosphine ligands can promote the LUMO energy levels. Third, the alkyl modification on phosphine ligands can improve the stabilities, which will obviously decrease the fabricating costs and elongate the working life of related devices.[19,20] Finally, quaternary phosphorus salt and silver-bearing compounds are traditional antibacterial materials, their hybridization will help improve antibacterial performance.[21,22] In this work, alkyl-bis-(triphenyl)phosphoniums with different spacer lengths (spacer n=2, 3, 4) were used as organic templates to obtain three new bromoargentate hybrids, ie, (1,2-DBTPP)(Ag_2Br_4) (**1**), {(1,3-DBTPP)$_2$(Ag_7Br_{11})]·CH_3CN·H_2O}$_n$ (**2**), and {[(1,4-DBTPP)(Ag_5Br_7)](CH_3CN)$_2$·H_2O}$_n$ (**3**) (1,2-DBTPP^{2+}=ethane-1,2-diyl-bis (triphenyl)phosphonium, 1,3-DBTPP^{2+}=propane-1,3-diylbis (triphenyl)phosphonium, 1,4-DBTPP^{2+}=butane-1,4-diylbis (triphenyl)phosphonium)). Their greenish blue luminescence, repeatable photocurrent responses and durable antibacterial activities correspond to the different spacer lengths, which could provide a theoretical guide for the design of new multifunctional materials.

Experimental Section

Materials and Physical Measurement

All chemicals were commercial products and used without further purification. Alkyl-bis-(triphenyl)phosphonium (1,2-DBTPP)Br_2, (1,3-DBTPP)Br_2 and (1,4-DBTPP)Br_2 were self-prepared. IR spectra were recorded on a Perkin-Elmer Spectrum-2000 FTIR spectrophotometer (4000–400 cm^{-1}) with powdered samples spread on a KBr plate. Elemental analyses for C, H and N were performed on a Vario MICRO elemental analyzer. Powder XRD patterns were obtained using a Philips X'Pert-MPD diffractometer with CuKα radiation (λ =1.54056 Å). The absorption spectra were measured on a Perkin-Elmer Lambda 900 UV/VIS spectrophotometer equipped with an integrating sphere at 293 K, and $BaSO_4$ plates were used as a reference. The optical gaps were calculated from reflectance spectra using the Kubelka −Munk function, $\alpha/s=(1-R)^2/2R$, where α is the absorption coefficient, s is the scattering coefficient, and R is the reflectance.[23] ^{1}H NMR and ^{13}C NMR spectra were recorded on a Bruker AVIII 400 spectrometer whose chemical shifts were reported in parts per million (ppm) downfield from tetramethylsilane. Fluorescence spectra were carried out on an Edinburgh FLS 980 Red PMT. The photocurrent experiments were performed on a CHI650 electrochemistry workstation with three-electrode systems using a Pt plate as the counter electrode and an Ag/AgCl electrode (3 M KCl) as the reference electrode. The morphologies of the devices were investigated by field emission scanning electron microscopy (SEM) spectrometer (Verios G4 UC), and the FE-SEM EDX is recorded by the EDAX Inc. Octane Elect Super.

Synthesis

Synthesis of Quaternary Phosphorus Salts

Three alkyl-bis-(triphenyl)phosphonium bromides (n=2: (1,2-DBTPP)Br_2, n=3: (1,3-DBTPP)Br_2, n=4: (1,4-DBTPP)Br_2) were prepared by a one-step alkylated reaction of triphenylphosphine with 1.2-dibromoethane, 1.3-dibromopropane and 1.4-dibromobutane in the DMF solvent according to the literature (Scheme S1).[24] The detailed synthesis process, ^{1}H NMR and ^{1}P NMR spectra can be seen in Figure S1 in the supplementary data.

Synthesis of (1,2-DBTPP)(Ag_2Br_4) (1): 1 was prepared by solution evaporation method. (1,2-DBTPP)Br_2 (0.0768 g, 0.1 mmol) and AgBr (0.0183 g, 0.1 mmol)

were dissolved in 20 mL acetonitrile with the suspension obtained. Afterwards, a small amount of NaBr solid was added slowly until the solution became clear. In addition, the resultant solution was kept stirring for 3 h at room temperature. The resultant solution was filtered, and the filtrate liquor was covered with a cling film at room temperature for slower evaporation. Colorless transparent block crystals were obtained after the growth period of 5 days. Yield: 40.3% (0.0210 g, based on Ag). Anal. Cald. for $C_{38}H_{34}Ag_2Br_4P_2$ (1087.93): calcd. C 41.92, H 3.13%; found C 41.72, H 3.16%. IR (cm^{-1}): 3050(w), 2855(w), 1580(w), 1476(m), 1098(s), 996(w), 733(s), 693(s), 490(s).

Synthesis of $\{(1,3\text{-DBTPP})_2(Ag_7Br_{11})]\cdot CH_3CN\cdot H_2O\}_n$ (2): The synthesis process of **2** was similar to that of **1**, except (1,3-DBTPP)Br_2(0.0726 g, 0.1 mmol) was used as starting material. Colorless transparent block crystals were obtained after 5 days. Yield: 51.2% (0.0206 g, based on Ag). Anal. Cald. for $C_{80}H_{73}Ag_7Br_{11}NOP_4$ (2824.26): calcd. C 34.02, N 0.49, H 2.60%; found C 34.34, N 0.54, H 2.66%. IR (cm^{-1}): 3060(w), 2920(w), 1580(w), 1493 (w), 1440(m), 1110(s), 992(w), 719(s), 690(s), 500(s).

Synthesis of $\{[(1,4\text{-DBTPP})(Ag_5Br_7)](CH_3CN)_2\cdot H_2O\}_n$ (3): 3 was prepared using the same procedure, except that (1,4-DBTPP) Br_2 (0.0837 g, 0.1 mmol) was used as the starting material. Colorless crystals were obtained after 6 days. The SEM diagrams of **1–3** can be seen in Figure S2. Yield: 38.5% (0.0139 g, based on Ag). Anal. Cald. for $C_{44}H_{46}Ag_5Br_7N_2OP_2$ (1779.48): calcd. C 29.70, N 1.57, H 2.61%; found C 30.36, N 1.63, H 2.71%. IR (cm^{-1}): 3060(w), 2920(w), 1580(s), 1443(s), 1120(s), 995(w), 854 (w), 720(w), 688(s), 490(s).

Electrode Preparation and Photocurrent Measurement

The solution coating method was adopted to prepare the electrodes of **1–3** in the photocurrent measurements.[25] The freshly synthesized powders (5 mg) were dissolved in DMF (0.3 mL) to obtain suspensions, which were dispersed evenly to produce slurries. The slurries were then spread onto precleaned ITO glasses (0.6×0.6 cm, 14 Ω per cm^2), whose side parts were previously covered using scotch tape. The working electrode was dried overnight under ambient conditions. A copper wire was connected to the side part of the working electrode using conductive tape. Uncoated parts of the electrode were isolated with epoxy resin. A 150 W high-pressure xenon lamp, located 15 cm away from the surface of the ITO electrode, was employed as a full-wavelength light source. The photocurrent experiments were performed on a CHI660 electrochemistry workstation in a three-electrode system, with the sample-coated ITO glass as the working electrode mounted on the window with an area of 0.25 cm^2, a Pt wire as the auxiliary electrode, and a Ag/AgCl electrode as the reference electrode. The supporting electrolyte solution was a 0.2 $mol\cdot L^{-1}$ sodium sulfate aqueous solution. The applied potential was 0.5 V for all measurements. The lamp was kept on continuously, and a manual shutter was used to block exposure of the sample to the light. The sample was typically irradiated at intervals of 10 s.

Antimicrobial Activity on *Streptococcus mutans* and *Candida albicans*

A *Streptococcus mutans* (*S. mutans*) strain (ATCC, 700610) and a *Candida albicans* (*C. albicans*, ATCC, 90029) strain, both from the American Type Culture Collection, were selected as the model pathogens for the antimicrobial activity experiments. After recovery on Brain Heart Infusion (BHI, for *S. mutans*) agar or Sabouraud dextrose agar (SDA, for *C. albicans*) plates, the microbes were cultured in 4 mL of BHI broth medium (for *S. mutans*) or Yeast Extract Peptone Dextrose (YPD) medium (for *C. albicans*) at 37°C for 24 h. For colony formation assay, 20 μL of microbial solution containing approximately 1×10^4 colony-forming units per mL (CFU/mL) of *S. mutans* or *C. albicans* was uniformly spread on a BHI agar plate or SDA plate, respectively, containing different concentrations of compounds. After incubation at 37°C for 48 h, the plates were photographed, and the number of colonies was counted. For growth curve assay, 200 μL of the suspension of *S. mutans* (10^4 CFU/mL) in BHI broth medium or *C. albicans* in YPD medium were added to each well of a 96-well plate, and different concentrations of the compounds were added to the wells. The growth of *S. mutans* or *C. albicans* was assessed using a Bioscreen C Automated Microbiology Growth Curve Analysis System (Turku, Finland) at 37°C under shaking at 200 rpm. The OD values at 600 nm were measured every hour for up to 36 or 48 h.

Computational Methods

First-principle density-functional theory (DFT) calculations were performed with the CASTEP program.[26,27]

The exchange correlation functional was described by a generalized gradient approximation (GGA) with Perdew−Burke−Ernzerhof functional for solids (PBE) scheme. A 3×2×2 Monkhorst-Pack grid with a total number of 6 k points in the irreducible Brillouin zone and 45 empty bands was adopted. The number of plane waves included in the basis was determined by a cutoff energy E_c of 435.4 eV. The other parameters and convergent criteria were the default values of CASTEP code.

X-Ray Crystallography

The intensity data of **1–3** were collected on a Bruker APEX II diffractometer using graphite-monochromated MoKα radiation (λ = 0.71073 Å) at room temperature, during which the *Lp* factor corrections and multiscan absorption corrections were applied. The structure was solved by direct methods with SHELX-97 program and refined by full-matrix least-squares techniques on F^2 with SHELXL-97 program.[28,29] For all nonhydrogen atoms, anisotropical refinements were carried out. All hydrogen atoms attached to carbon atoms were geometrically placed. Crystal parameters of three compounds are summarized in Table 1. Selected bond lengths and angles are listed in Table S1, ***π–π*** stacking interactions and C–H···π interactions are given in Table S2 and S3. Crystallographic data have been deposited with the Cambridge Crystallographic Data Center as supplementary publication number CCDC-1818452 (**1**), 1818423 (**2**), and 1590456 (**3**). These data can be obtained free of charge from The Cambridge Crystallographic Data Centre *via* www.ccdc.cam.ac.uk/data_request/cif.

Results and Discussion

Structural Description

Compounds **1–3** are composed of bromoargentate anions ($(Ag_2Br_4)^{2-}$ dimers for **1**, $(Ag_7Br_{11})_n^{4n-}$ chains for **2** and $(Ag_5Br_7)_n^{2n-}$ chains for **3**) and corresponding alkyl-bis-(triphenyl)phosphonium cationic templates, among which hydrogen bonds contribute to the structural stabilization. The $(Ag_2Br_4)^{2-}$ in **1** is defined by two edge-sharing $AgBr_3$ triangles, giving two terminal (Br(2), Br(2)$^{\#1}$, #1: -x, 1-y, -z) and two bridged Br ions (Br(1), Br(1)#1, Figure 1A). The distance of terminal bromine and silver (2.5356(11) Å) is slightly shorter than that of bridging atoms (2.6632(11) Å, Table S2). Furthermore, the parallelograms defined by four atoms Ag(1), Br(1), Ag(1)$^{\#1}$ and Br(1)$^{\#1}$ are coplanar. The $(Ag_2Br_4)^{2-}$ dimers were seldom documented.[30–32] The Ag-Ag distance of 3.0253(14) Å is shorter than the sum of the van der Waals radii of silver (3.44 Å), hinting at the presence of an argentophilicity interaction.[6,34] The configuration of the $(1,2\text{-DBTPP})^{2+}$ cation in **1** is unfolding based on the P(1)-C(19)-C(19)$^{\#1}$ angle (115.99°) (Figure 1B). C-H···Br hydrogen bonds between $(1,2\text{-DBTPP})^{2+}$ cations and $(Ag_2Br_4)^{2-}$ dimers contribute to the formation of a 2-D layer (Figure 1C, Table S3). Due to the tetrahedral geometry of the PPh_3 moiety, no benzene-benzene π−π stacking interactions can be detected.

The $(Ag_7Br_{11})_n^{4n-}$ of **2** is a straight chain built from cubane-like Ag_4Br_4 nodes, $AgBr_4$ tetrahedrons and $AgBr_3$ triangles (Figure 2A), which has not been documented in bromoargentate systems. The distorted cubane-like Ag_4Br_4 core is an iso-structure of Ag_4I_4 cubane, which has been commonly observed in iodoargentates, for example, 1-D chains ($[(APHEN\text{-}H)_2(Ag_4I_6)]_n$),[34] 2-D layers ($\{[PC]_2[Ag_4I_6]\}_n$),[35] and 3-D open frameworks ($\{[BCP]_2[Ag_4I_6]\}_n$).[36] In **2**, each cubane-like Ag_4Br_4 core connects with two neighboring AgI_4 tetrahedrons via an edge-sharing mode (defined by Br(3)-Br(7)) to give a Ag_6Br_{10} unit; furthermore, the Ag_6Br_{10} unit links with the $Ag(4)Br_3$ triangle to generate a Ag_6Br_{11} building block. Neighboring Ag_6Br_{10} building blocks are extended into a 1-D chain via vertex (defined by Br(6))-sharing mode (Figure 2A). Consequently, two kinds of coordinated geometries of Ag centers can be found, including tetrahedral (Ag(1), Ag(2), Ag(3), Ag(5)) and planar triangle (Ag(4)). Specifically, the $Ag(3)Br_4$ tetrahedron is highly distorted with Ag-Br distances of 2.617(3)−905(3) Å. Abundant Ag···Ag interactions with separations of 3.026(3) −3.323(4) Å are observed, indicating the presence of strong argentophilic interactions (Table S2). The bond lengths of the $(1,3\text{-DBTPP})^{2+}$ cation are within normal range, and the bond angle in the methane (C(19)-C(20)-C(19)$^{\#1}$) is 107.16°, suggesting its folded configuration (Figure 2B). There are no π−π stacking interactions in the lattice, but C-H···Br hydrogen bonds contribute to the formation of a quasi-3-D network (Figure 2C). In addition, solvent molecules CH_3CN and H_2O also stack in the lattice.

Table 1 PL Data of 1–3 at Room Temperature

Compound	λ_{ex}(nm)	λ_{em}(nm)	Φ (%)
1	320	488	6.24
2	350	513	6.21
3	340	490	6.26

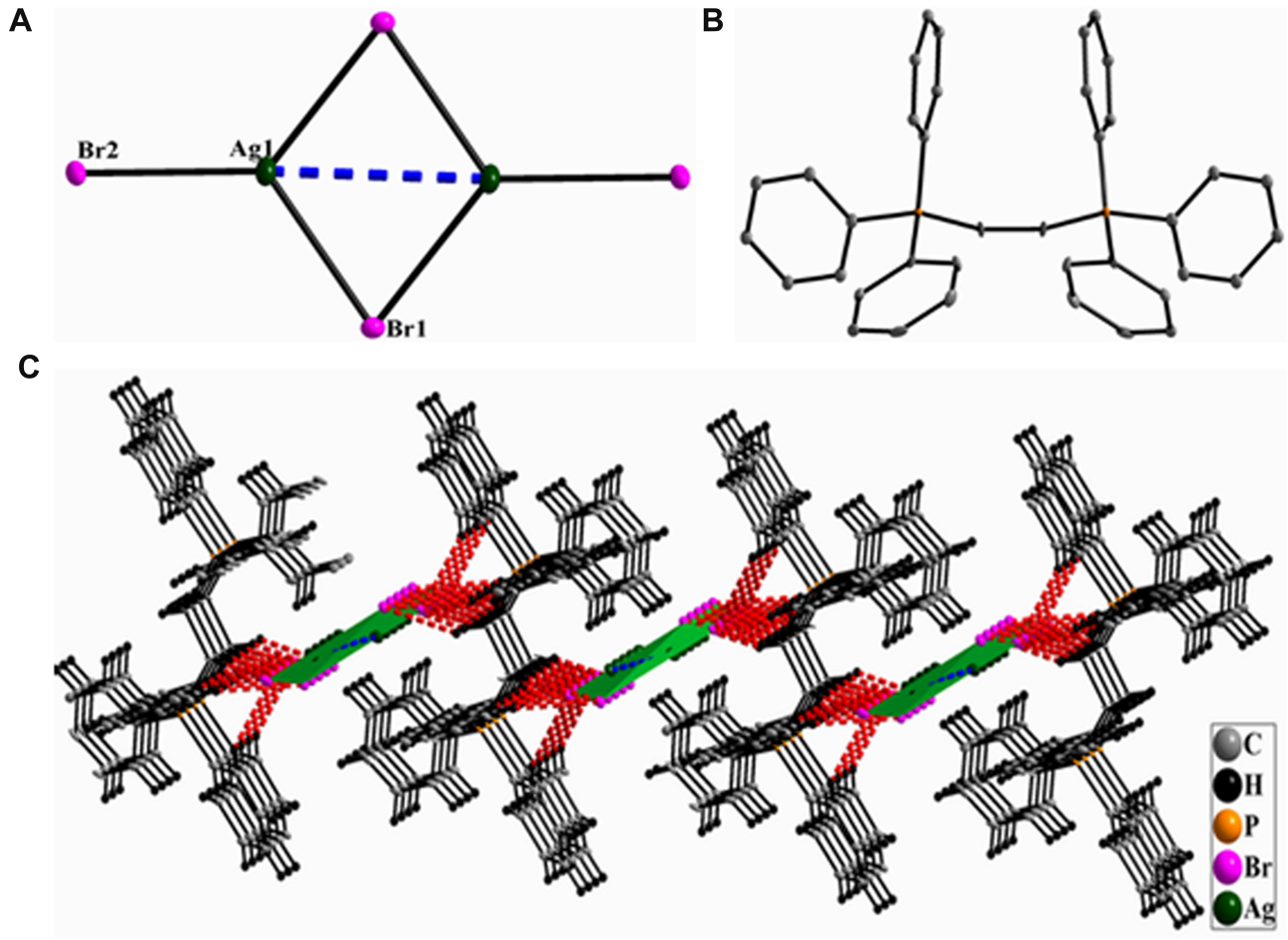

Figure 1 (**A**) The structure of the $(Ag_2Br_4)^{2-}$ anion; (**B**) the configuration of the $(1,2\text{-DBTPP})^{2+}$ cation (H were omitted for clarity); (**C**) packing diagram showing C–H···Br hydrogen bonds.

The $(Ag_5Br_7)_n^{2n-}$ chain takes on a zigzag configuration based on much more complicated Ag···Ag interactions, which is the iso-structure of the $(Ag_5I_7)_n^{2n-}$ chain in $\{[Et_3N(CH_2)_6NEt_3][Ag_5I_7]\}_n$.[37] The building block is a Ag_5Br_{10} unit in which all Ag centers adopt an Br_4 donor set and tetrahedral geometries. The Ag_5Br_0 building block could be described as the edge-sharing of five $AgBr_4$ tetrahedrons. Adjacent Ag_5I_{10} building blocks are extended into a 1-D zigzag chain along the a-axis via an edge-sharing mode (Figure 3A). Strong Ag···Ag interactions could be found with distances ranging from 3.0289(13) to 3.1918(14) Å. In Particular, a μ_5-Br(3) is found in this polymeric chain, which is seldom seen in haloargentate compounds. The configuration of $(1,4\text{-DBTPP})^{2+}$ cation is determined from the bond angles in methene (111,73 and 116.915°, Figure 3B). Similarly, C-H···Br hydrogen bonds contribute to the formation of quasi-3-D network (Table S3, Figure 3C), and additional CH_3CN and H_2O molecules stack in the cavities. This work again proves the rigidity/flexibility competition in haloargentates/organic hybrids, ie, when the spacer is short, the alkyl flexibility dominates in the structural stabilization, but when the spacer is longer, to some extent, the benzene rigidity plays a more important role.[7] In this work, when spacer n=2, only simple $(Ag_2Br_4)^{2-}$ dimmer is given, but when spacer n=3 and 4, more complicated $(Ag_7Br_{11})_n^{4n-}$ and $(Ag_5Br_7)_n^{2n-}$ chains are produced.

Stabilities in Water

The stabilities of functional materials in solvents will determine their real applications.[15,38] In this work, alkyl-bis-(triphenyl)phosphoniums with different spacer lengths might affect their water stability. Most of the functional properties of this work were conducted in water; therefore, their stabilities in water were studied. During the water stability measurements, the freshly prepared crystalline samples of **1**–**3** were ground as fine powders and soaked in deionized water at room temperature with different time

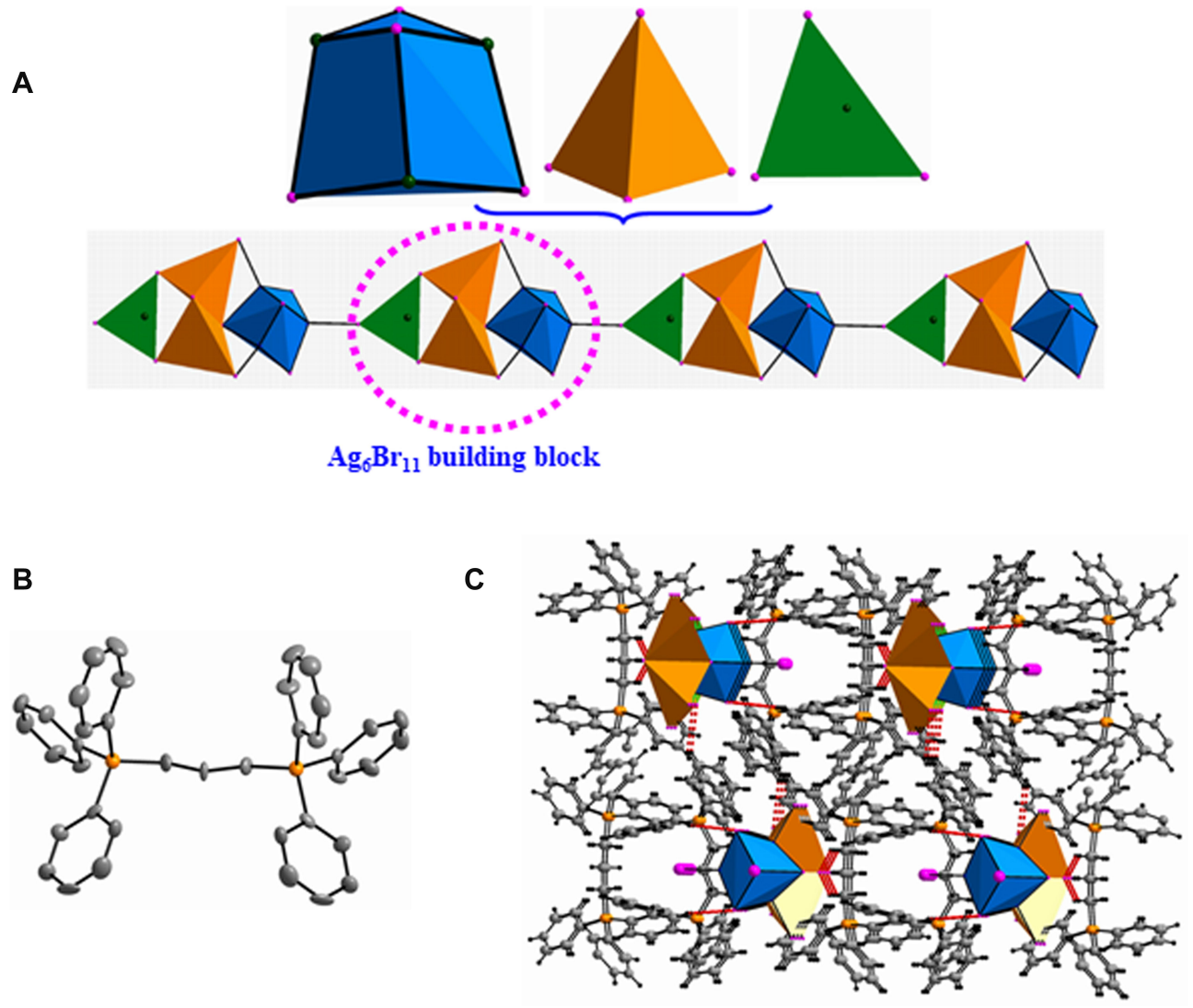

Figure 2 (**A**) The 1-D $(Ag_7Br_{11})_n^{4n-}$ straight chain built from cubane-like Ag_4Br_4 nodes, $AgBr_4$ tetrahedrons and $AgBr_3$ triangles; (**B**) the configuration of the $(1,3\text{-DBTPP})^{2+}$ cation (H were omitted for clarity); (**C**) quasi-3-D network based on C–H···Br hydrogen bonds.

intervals. Afterwards, the samples were centrifuged and dried at 40°C, and PXRD experiments were conducted to check their phases. The phase purities of bulk compounds **1**–**3** have been verified by powder X-ray diffraction (PXRD), in which the peaks of the as-synthesized samples are in good agreement with the simulated peaks (Figure 4). Furthermore, the water stability measurements under different soaking times (1, 3 and 5 days) imply that the crystal structures of **1**–**3** can persist after soaking in water for 3 days. After soaking for 5 days, **1** will collapse to some extent judging from its PXRD pattern (Figure 4A). However, **2** and **3** still maintain their structures (Figure 4B and C), implying that they have better water stabilities than **1**. This trend suggests that the longer spacer lengths will result in better water stabilities, which might be induced by their better flexibilities when facing the attack of solvents. This phenomenon again proves the conclusion that in the quaternary phosphorus-containing hybrids, a longer alkyl chain can give rise to better water stability.[15] In addition, the thermal stability of **3** was also determined, which could not decompose until 320°C (Figure S3). The good water/thermal stabilities will be beneficial for their long-term antibacterial performances.

Optical Diffuse-Reflection Spectra and Photoluminescence

Solid-state optical diffuse-reflection spectra of **1**–**3** were recorded from powder samples at room temperature (Figure 5A). They exhibit intense adsorption in the

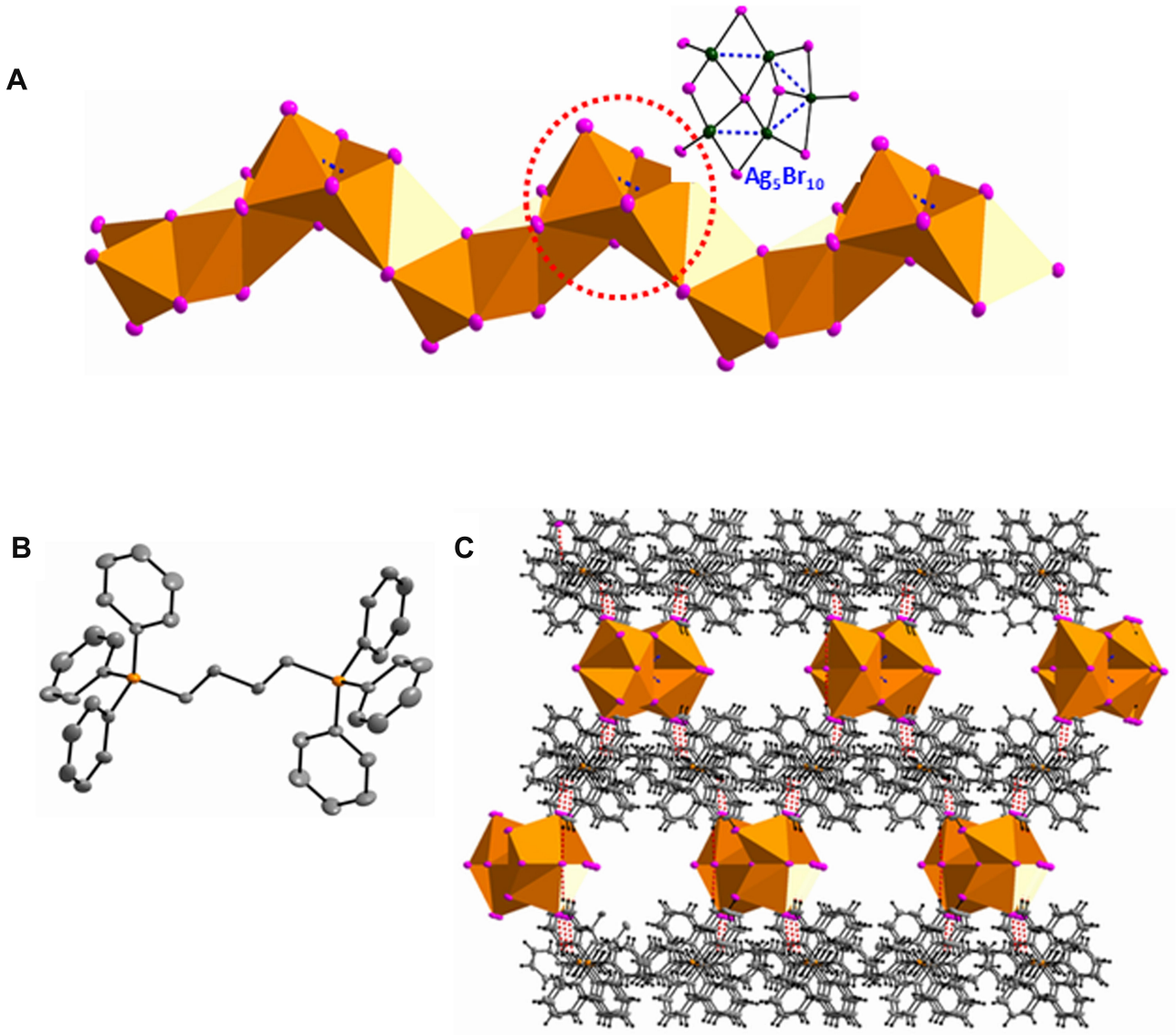

Figure 3 (**A**) The 1-D zigzag $(Ag_5Br_7)_n^{2n-}$ chain built from the Ag_5Br_{10} building block; (**B**) the configuration of the $(1,4\text{-DBTPP})^{2+}$ cation (H were omitted for clarity); (**C**) quasi-3-D network based on C–H···Br hydrogen bonds.

ultraviolet zone (281 nm for **1**, 301 nm for **2** and 291 nm for **3**). Comparably, the adsorption peaks of organic quaternary phosphorus salts generally appear at approximately 330 nm, corresponding to the n–π*/π–π* transitions of phenyl groups in the phosphonium core.[15] Therefore, compared with free phosphonium, the corresponding electronic transitions of **1**–**3** can definitely be attributed to the ligand-centered n–π*/π–π* transitions of phosphine ligands.[39] There are blanks in the range of 350–800 nm, suggesting the absence of ligand-to-ligand charge transfer (LLCT) and charge transfer between inorganic bromoargentates and organic moieties.[40] These correspond to the absence of π–π and C–H···π interactions in their lattices, as indicated by structural analysis. Solid-state UV–Vis diffuse spectra of **1**–**3** calculated from the diffuse reflectance data by using the Kubelka–Munk function is plotted in Figure S4. The band gaps can be estimated as 3.60, 3.55 and 3.70 eV, which indicate that **1** and **2** are wide-gap semiconductors and **3** is generally an insulator. The wide band gaps are commonly observed in organic/bromoargentate hybrids.[41] Compared with the gap of bulk AgBr (2.81 eV), obvious blueshifts have occurred. More importantly, the conclusion could be drawn that in the phosphonium-containing hybrids, the gaps will be dominated by organic phosphonium cores.

One-photon photoluminescence spectra of **1**–**3** measured at room temperature in the solid state are shown in Figure 5B (exited, emission peaks and quantum yields are

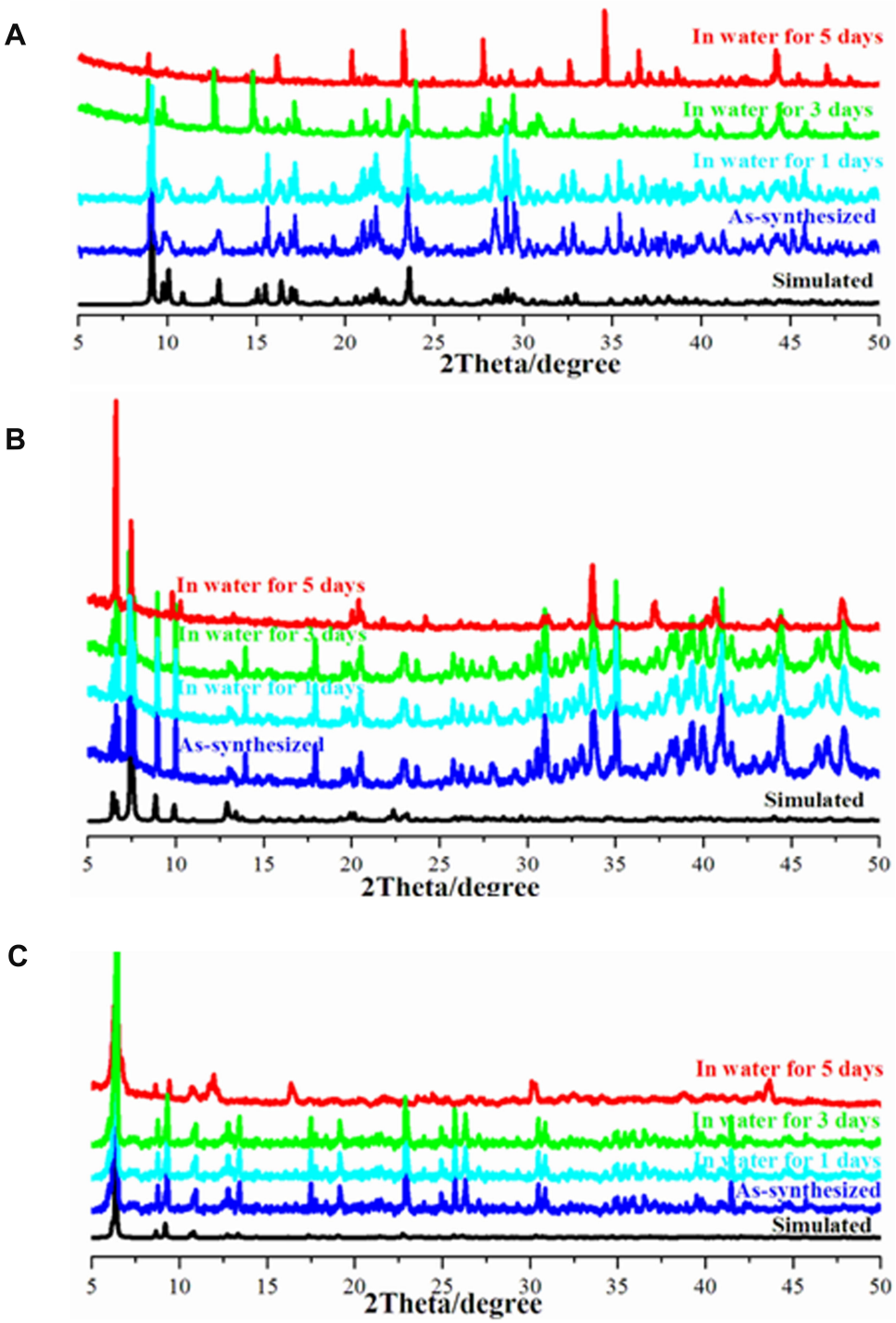

Figure 4 The PXRD patterns of 1 (**A**), 2 (**B**) and 3 (**C**) soaked in water for different times.

summarized in Table 1). Generally, the three hybrids generated the same single greenish blue emissions in the solid state at room temperature when excited at 320–350 nm, with luminescent colors illustrated in the CIE-1931 profiles (Figure 5B-C). As reported by literature, free organic quaternary phosphorus iodide (Ph_3P*n*-Bu·I) also exhibits cyan emission (at 485 nm) under excitation at 340 nm, which was attributed to the photoinduced charge transfer from the iodine anion to the phosphonium core.[15] Compared with the emission of phosphonium iodide, compound **2** with spacer length n=3 presents the largest red-shift of approximately 28 nm, and conclusions could be

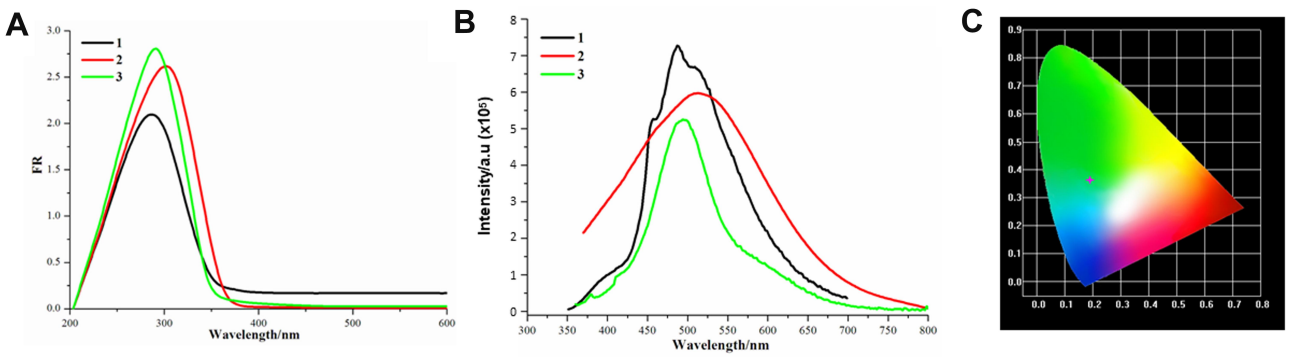

Figure 5 (**A**) Solid state electronic spectra; (**B**) emission spectra at room temperature with CIE-1931 chromaticity of 1–3. (**C**) CIE-1931 chromaticity diagram.

drawn that these greenish blue emissions all stem from the photoinduced charge transfer from bromoargentates to phosphoniums. Moreover, their quantum yields are generally the same (ranging from 6.21 to 6.26%). Their photoluminescence implies their potential application as biological imaging or cancer therapy compounds.[42,43]

Photocurrent Response Performances

Photoinduced current generation can be potentially used in molecular switches, information storage, and so on, and has been detected in organic/metal halides hybrids.[6,44] Photocurrent response performances have also been executed on **1**–**3** using typical methods, in which three electrode photo/electrochemical cell systems were adopted (a sample-modified ITO electrode as a working electrode, a Pt wire as an auxiliary electrode and a Ag/AgCl electrode as a reference electrode). All the experiments were conducted in Na_2SO_4 aqueous solutions under the illumination from a 150 W Xe arc lamp with on–off cycles (an on-off interval of 20 s). Under repetitive irradiation, repeatable photocurrents with rapid responses can be detected on all compounds (Figure 6A). The photocurrent of **1** and **2** first decreases and then stabilizes after five cycles, but the current of **3** is steady without decay. Their photocurrents stabilize at approximately 1.10×10^{-7}(for **1** and **2**) and 1.30×10^{-7} A (for **3**), which are weaker than those of viologen-containing compounds, such as $(MV)_2[Li_4(L)_2(H_2O)_6]$ and $MV[Ni(4\text{-pedt})_2]_2$.[45] It is universally accepted that the pure organic-coated system did not show any photocurrent response,[46] so the bromoargentate/phosphonium donor–acceptor systems are responsible for the photocurrent generation in this work. Consequently, its photoinduced current generation mechanism is given: first, the photosensitive phosphonium cations are irradiated to generate the $(Ph_3\text{-}R\text{-}Ph_3)^{2+}$• radicals, and at the same time, $Ag_xBr_y^{(y-x)-}$ donors also transfer electrons to phosphoniums with production of $Ag_xBr_y^{(y-x)-}$• radicals. Second, the $(Ph_3\text{-}R\text{-}Ph_3)^{2+}$• radicals transfer their electrons to the ITO electrodes with reproduction of the $(Ph_3\text{-}R\text{-}Ph_3)^{2+}$ acceptor. As a result, an electron conductive pair of $Ag_xBr_y^{(y-x)-}$•–$(Ph_3\text{-}R\text{-}Ph_3)^{2+}$• is responsible for their repeated currents (Figure 6B). This process can also be verified by the components of the tops of VBs (Ag-4d, Br-4p) and the bottoms of CBs (p-π* anti-bonding orbital of the quaternary phosphorus) in the PDOS of **1** (Figure 6C). As indicated by this mechanism, the stronger C-H···Br hydrogen bond in **3** (the shorter H···Br distance of 2.74 Å, Table S3) can facilitate the electronic transfer; as a result, a relative higher current intensity in **3** can be found.

Antimicrobial Performance Against *S. mutans* and *C. albicans*

Silver, quaternary ammoniums are traditional antibacterial materials to inhibit or reduce the growth of detrimental bacteria.[47] *Streptococcus mutans* (*S. mutans*) is a commensal microorganism found in the human oral cavity and the primary causative agent of dental caries.[48] In this work, the antibacterial activity of **2** and **3** were tested against *S. mutans* according to the standard antibacterial test of insoluble antimicrobials, and the results are shown in Figure 7. Interestingly, the presence of **2** and **3** can effectively inhibit the growth of *S. mutans*. The antimicrobial rate can reach 90% for **2** and 68% for **3** when the bromoargentate hybrids' concentrations are 100 μg/mL (Figure 7A and B), and the bacteria did not grow for 36 h with 40 μg/mL of **2** or 50 μg/mL of **3** (Figure 7C and D). The minimum inhibitor concentration (MIC) is approximately 50 μg/mL according to the growth curves, which is comparable to and even better than the MIC of currently accessible silver-loaded zeolites (50–150 μg/mL) and AgBr/NPVP composites (approximately 100 μg/mL).[49] This improved antibacterial performance of quaternary

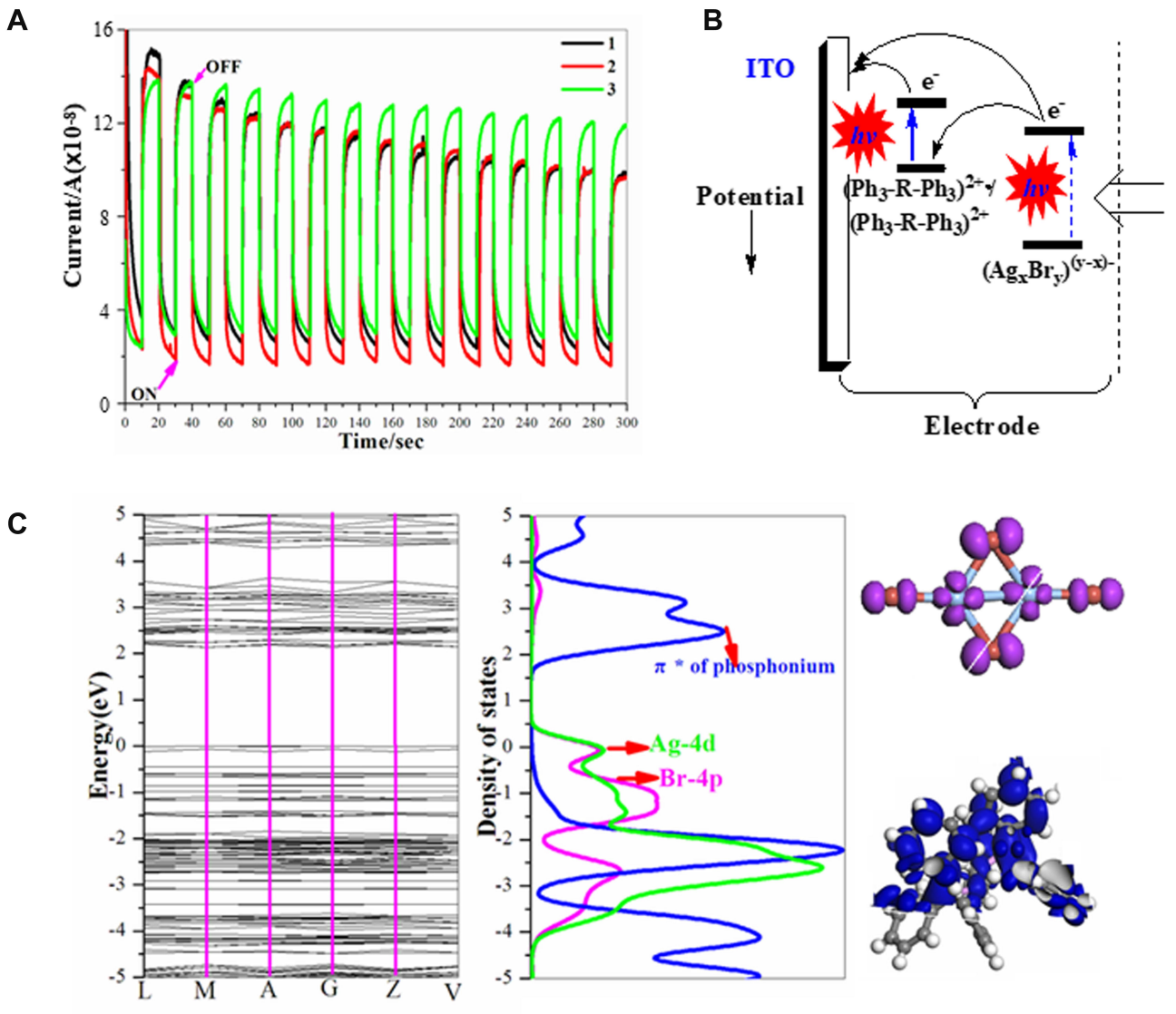

Figure 6 (**A**) Photocurrent curves, (**B**) photocurrent response mechanisms and (**C**) bond structure (left), projected density of states (pDOS, middle) and frontier orbitals (right) for 1.

phosphorus/bromoargentate hybrids can be assigned to the following aspects. First, the quaternary phosphorus moieties of hybrids can lead to the disruption of the cytoplasmic membranes of *S. mutans*.[50] Second, the sustained and slow releases stemming from the exceedingly low solubility of bromoargentates in **2** and **3** are beneficial for efficient inhibition of bacterial growth and are consistent with their good solution stabilities.[51] The sustained release of biocidal Ag^+ ions can deactivate cellular enzymes and DNA by coordinating electron-donating groups and causing pits in bacterial cell walls, and as a result, lead to increased permeability and cell death. *Candida albicans* is one of the commonly seen yeasts in the human mouth and the main pathogen of denture stomatitis; the detection rate of dental plaque is 81.7%.[52] In the present study, we also tested the antifungal activity of these compounds on *C. albicans*. Interestingly, we found that compounds 2 and 3 showed strong antifungal activity, as shown in Figure 8. The inhibition rate was 80% for **2** and 57% for **3** when the bromoargentate hybrids' concentrations were 100 μg/mL (Figure 8A and B), and the fungi did not grow for more than 40 h with 200 μg/mL of **2** or **3** (Figure 8C and D). These results indicated that the bromoargentate hybrids possess excellent antimicrobial activities by inhibition the growth of *S. mutans* and *C. albicans*.

Conclusions

In summary, bromoargentate hybrids directed by (triphenyl) phosphonium-based quaternary phosphorus salts with

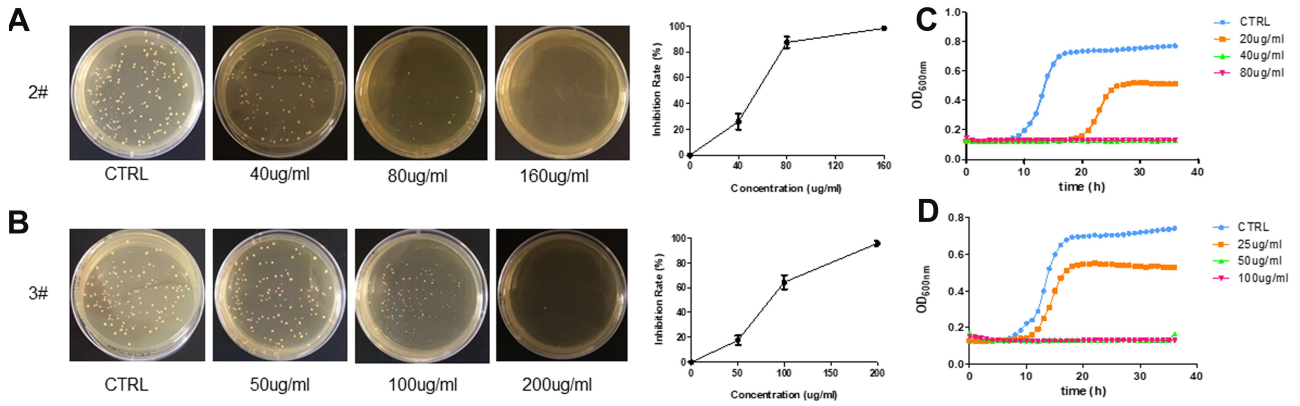

Figure 7 Antibacterial performance against *S. mutans*: images of the *S. mutans* colonies grown on BHI agar plates and the inhibition rate of 2 (**A**) and 3 (**B**); the growth curves of *S. mutans* with different concentrations of 2 (**C**) and 3 (**D**).

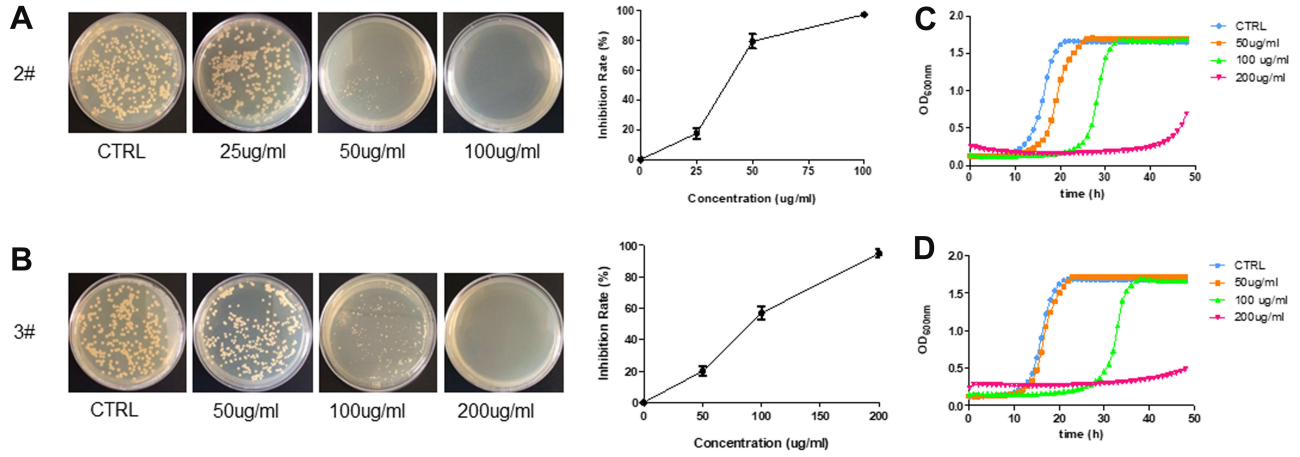

Figure 8 Antifungal activity against *C. albicans:* images of the colonies grown on YPD agar plates and the inhibition rate of 2 (**A**) and 3 (**B**); the growth curves of *C. albicans* with different concentrations of 2 (**C**) and 3 (**D**).

different spacer lengths (n=2, 3, 4) have been prepared. The $(Ag_7Br_{11})_n^{4n-}$ chain in **2** is a new type of 1-D bromoargentate chain constructed from Ag_7Br_{12} units, but the zigzag $(Ag_5Br_7)_n^{2n-}$ chain in **3** is based on Ag_5Br_9 units. Interestingly, with the elongation of spacer n from 2 to 4, argentophilicity interactions are weakened, and the hydrogen bonds are strengthened. Consequently, better water stabilities and enhanced photocurrents are observed. Furthermore, high inhabitation rates against *S. mutans* and *C. albicans* can be observed. Overall, the elongation of the spacer lengths can give rise to better functional properties, which could provide a theoretical guide for the design of new multifunctional materials.

Funding

This work was financially supported by Joint Funds for the Innovation of Science and Technology of Fujian Province (Grant number: 2018Y9033), Research Project from the Department of Science and Technology of Fujian Province (Grant number: 2017Y0040) and Key Laboratory Foundation of Stomatology of Fujian Province University (Grant number: 2019kq03).

Disclosure

The authors declare no competing financial interest.

References

1. Zhao Y, Zhu K. Organic–inorganic hybrid lead halide perovskites for optoelectronic and electronic applications. *Chem Soc Rev*. 2016;45(3):655–689. doi:10.1039/C4CS00458B
2. Gratzel M. The rise of highly efficient and stable perovskite solar cells. *Acc Chem Res*. 2017;50:487–491. doi:10.1021/acs.accounts.6b00492
3. Smith MD, Karunadasa HI. White-light emission from layered halide rerovskites. *Acc Chem Res*. 2018;51(3):619–627. doi:10.1021/acs.accounts.7b00433

4. Bi WH, Louvain N, Mercier N, et al. A switchable NLO organic-inorganic compound based on conformationally chiral disulfide molecules and Bi(III)I5Iodobismuthate networks. *Adv Mater*. 2008;20:1013–1017. doi:10.1002/adma.200701753
5. Wang YK, Zhao LM, Fu YQ, et al. Combination of N-arylstilbazolium organic nonlinear optical chromophores with iodoargentates: structural diversities and optical properties. *Cryst Growth Design*. 2018;18 (7):3827–3840. doi:10.1021/acs.cgd.8b00033
6. Wang DH, Zhao LM, Lin XY, et al. Iodoargentate/iodobismuthate-based materials hybridized with lanthanide-containing metalloviologens: thermochromic behaviors and photocurrent responses. *Inorg Chem Front*. 2018;5:1162–1173. doi:10.1039/C7QI00755H
7. Li HH, Xing YY, Lian ZX, et al. Rigidity/flexibility competition in organic/iodoargentate hybrids: a combined experimental and theoretical Study. *Cryst Eng Comm*. 1721–1728;2013(15).
8. Yu TL, Guo YM, Wua GX, et al. Recent progress of d^{10} iodoargentate(I)/iodocuprate(I) hybrids: structural diversity, directed synthesis, and photochromic/thermochromic properties. *Coord Chem Rev*. 2019;397:91–111.
9. Li HH, Chen ZR, Sun LG, et al. Two iodoargentate hybrid coordination polymers induced by transition-metal complexes: structures and properties. *Cryst Growth Design*. 2010;10:1068–1073. doi:10.1021/cg900476m
10. Yu T, Fu Y, Wang Y, Hao P, Shen J, Fu Y. Hierarchical symmetry transfer and flexible charge matching in five $[M(phen)_3]^{2+}$ directed iodoargentates with 1 to 3D frameworks. *Cryst Eng Comm*. 2015;17:8752–8761. doi:10.1039/C5CE01692D
11. Li L, Chen H, Qiao YZ, Niu YY. The subtle effect of methyl substituent in C2-symmetric template on the formation of halocluster hybrids. *Inorg Chim Acta*. 2014;409:227–232. doi:10.1016/j.ica.2013.09.029
12. Sharutin VV, Sharutina OK, Senchurin VS, Neudachina AN. Synthesis and structure of silver complexes $[Ph_3(i\text{-}Pr)P]^{+}2[Ag_2I_4]^{2-}$ and $[Ph_3MeP]^{+}[Ag_3I_4]_n^{n-}$. *Russ J Gen Chem*. 2016;86:1653–1658. doi:10.1134/S1070363216070203
13. Bowmakera GA, Bruceb MI, Skeltonc BW, Somersc N, Whitec AH. Structural and spectroscopic studies of halocuprate(I) and haloargentate(I) complexes $[M_2X_nX'_{4-n}]^{2-}$. *Z. Anorg. Allg. Chem*. 2007;633(7):1024–1030. doi:10.1002/zaac.200700051
14. Jaafar M, Liu X, Dielmann F, et al. Synthesis, structure and spectroscopic properties of bis(triphenylphosphane)iminium (chlorido)(cyanido)argentates(I). *Inorg Chim Acta*. 2016;443:45–50. doi:10.1016/j.ica.2015.12.018
15. Zhang WT, Liu JZ, Liu JB, et al. Quaternary phosphorus-induced iodocuprate(I)-based hybrids: water stabilities, tunable luminescences and photocurrent responses. *Eur J Inorg Chem*. 2018;2018 (38):4234–4244. doi:10.1002/ejic.201800813
16. Hashimoto M, Igawa S, Yashima M, Kawata I, Hoshino M, Osawa M. Highly efficient green organic light-emitting diodes containing luminescent three-coordinate copper(I) complexes. *J Am Chem Soc*. 2011;133:10348–10351. doi:10.1021/ja202965y
17. Zhang Q, Komino T, Huang S, Matsunami S, Goushi K, Adachi C. Triplet exciton confinement in green organic light-emitting diodes containing luminescent charge-transfer Cu(I) complexes. *Adv Funct Mater*. 2012;22(11):2327–2336. doi:10.1002/adfm.201101907
18. Chen XL, Yu RM, Zhang QK, et al. Rational design of strongly blue-emitting cuprous complexes with thermally activated delayed fluorescence and application in solution-processed OLEDs. *Chem Mater*. 2013;25:3910–3920. doi:10.1021/cm4024309
19. Liu GN, Zhao RY, Xu H, et al. The structures, water stabilities and photoluminescence properties of two types of iodocuprate(i)-based hybrids. *Dalton Trans*. 2018;47:2306–2317. doi:10.1039/C7DT04558A
20. Liu W, Zhu K, Teat SJ, et al. Achieving robust, strongly luminescent and highly dispersible hybrid materials by combining ionic and coordinate bonds in molecular crystals. *J Am Chem Soc*. 2017;139 (27):9281–9290. doi:10.1021/jacs.7b04550
21. Yuan Y, Sun F, Zhang F, et al. Targeted synthesis of porous aromatic frameworks and their composites for versatile, facile, efficacious, and durable antibacterial polymer coatings. *Adv Mater*. 2013;25:6619–6624. doi:10.1002/adma.201301955
22. Tatarinov DA, Kuznetsov DM, Voloshina AD, et al. Synthesis of 2-(2-hydroxyaryl)alkenylphosphonium salts from phosphine oxides via ring-closing ring-opening approach and their antimicrobial evaluation. *Tetrahedron*. 2016;72(51):8493–8501. doi:10.1016/j.tet.2016.11.023
23. Kubelka P, Munk F. An article on optics of paint layers *Z. Tech Phys*. 1931;12:593–601.
24. Patil RA, Talebi M, Xu C, Bhawal SS, Armstrong DW. Synthesis of thermally stable geminal dicationic ionic liquids and related ionic compounds: an examination of physicochemical properties by structural modification. *Chem Mater*. 2016;28(12):4315–4323. doi:10.1021/acs.chemmater.6b01247
25. Hou JL, Luo W, Guo Y, et al. Titanium oxo cluster with six peripheral ferrocene units and its photocurrent response properties for saccharides. *Inorg Chem*. 2017;56:6451–6458. doi:10.1021/acs.inorgchem.7b00522
26. Segall MD, Lindan PJD, Probert MJ, et al. First-principles simulation: ideas, illustrations and the CASTEP code. *J Phys Condens Matter*. 2002;14:2717–2744.
27. Clark SJ, Segall MD, Pickard CJ, et al. First principles methods using CASTEP *Z Kristallogr. Cryst Mater*. 2005;220:567–667. doi:10.1524/zkri.220.5.567.65075
28. Sheldrick GM. *SHELXS-97: Program for Crystal StructureSolution*. Göttingen, Germany: Göttingen University; 1997.
29. Sheldrick GM. *SHELXL-97: Program for the Refinement of Crystal Structures*. Göttingen, Germany: Göttingen University; 1997.
30. Liu Q-X, Yang X-Q, Zhao X-J, et al. Macrocyclic dinuclear silver(I) complexes based on bis(N-heterocyclic carbene) ligands: synthesis and structural studies. *CrystEngComm*. 2010;12(7):2245–2255. doi:10.1039/b919007d
31. Saito S, Saika M, Yamasaki R, Azumaya I, Masu H. Synthesis and structure of dinuclear silver(I) and palladium(II) complexes of 2,7-Bis(methylene)naphthalene-bridged Bis-NHeterocyclic carbene ligands. *Organometallics*. 2011;30:1366–1373. doi:10.1021/om1008583
32. Keske EC, Zenkina OV, Wang R, Crudden CW. Synthesis and structure of silver and rhodium 1,2,3-Triazol-5-ylidene mesoionic carbene complexes. *Organometallics*. 2012;31:456–461.
33. Li HH, Huang SW, Lian ZX, Liu JB, Wang M, Chen ZR. Incorporating rare earth metal complexes and conjugated organic cations into polymeric iodoargentate: structures and properties of two hybrid iodoargentates. *Z Anorg Allg Chem*. 2012;638:851–855. doi:10.1002/zaac.201100477
34. Li HH, Wu JX, Dong HJ, Wu YL, Chen ZR. A combined experimental and theoretical study of an semi-conductive iodoargentate hybrid induced by large conjugate cation. *J Mol Struct*. 2011;987 (1–3):180–185. doi:10.1016/j.molstruc.2010.11.077
35. Shen JJ, Zhang CF, Yu TL, An L, Fu YL. Structural and functional modulation of five 4-cyanopyridinium iodoargentates built up from cubane-like Ag_4I_4 nodes. *Cryst Growth Des*. 2014;14:6337–6342.
36. Hao PF, Qiao YR, Yu TL, Shen JJ, Dai DT, Fu YL. Three iodocuprate hybrids symmetrically modulated by positional isomers and the chiral conformation of N-benzyl-methylpyridinium. *RSC Adv*. 2016;6:53566–53572. doi:10.1039/C6RA08692F

37. Li HH, Chen ZR, Li JQ, Huang CC, Zhang YF, Jia GX. Role of spacers and substituents in self-assembly process: syntheses and characterization of three novel silver(I)/iodine polymers. *Cryst. Growth&Des*. 2006;6:1813–1820.
38. Hei X, Liu W, Zhu K, et al. Blending ionic and coordinate bonds in hybrid semiconductor materials: a general approach toward robust and solution-processable covalent/coordinate network structures. *J Am Chem Soc*. 2020;142(9):4242–4253. doi:10.1021/jacs.9b13772
39. Huang CH, Wen M, Wang CY, et al. A series of pure-blue-light emitting Cu(i) complexes with thermally activated delayed fluorescence: structural, photophysical, and computational studies. *DaltonTrans*. 2017;46(5):1413–1419. doi:10.1039/C6DT03965K
40. Xu LJ, Wang JY, Zhu XF, Zeng XC, Chen ZN. Phosphorescent cationic Au_4Ag_2 alkynyl cluster complexes for efficient solution-processed organic light-emitting diodes. *Adv Funct Mater*. 2015;25:3033–3042.
41. Zhang RC, Wang JJ, Yuan BQ, et al. Syntheses and characterization of chiral zeolitic silver halides based on 3-rings. *Inorg Chem*. 2016;55(21):11593–11599. doi:10.1021/acs.inorgchem.6b02121
42. Jiang YY, Huang JG, Zhen X, et al. A generic approach towards afterglow luminescent nanoparticles for ultrasensitive in vivo imaging. *Nat Commun*. 2019;10(1−10):2064. doi:10.1038/s41467-019-10119-x
43. Zhen X, Xie C, Jiang YY, Ai XZ, Xing BG, Pu KY. Semiconducting photothermal nanoagonist for remote-controlled specific cancer therapy. *Nano Lett*. 2018;18:1498–1505. doi:10.1021/acs.nanolett.7b05292
44. Zhao LM, Zhang WT, Song KY, et al. Lead-carboxylate/polyiodide hybrids constructing from halogen bonding and asymmetric viologen: structures, visible-light-driven photocatalytic properties and enchanced photocurrent responses. *Cryst Eng Comm*. 2018;20:2245–2252. doi:10.1039/C8CE00120K
45. Huang YD, Huo P, Shao MY, et al. A new type of charge-transfer salts based on tetrathiafulvalene–tetracarboxylate coordination polymers and methyl viologen. *Inorg Chem*. 2014;53:3480–3487. doi:10.1021/ic402926n
46. Shen WC, Huo P, Huang YD, Yin JX, Zhu QY, Dai J. Photocurrent responsive films prepared from a nickel-dithiolate compound with directly bonded pyridyl groups. *RSC Adv*. 2014;4:60221–60226. doi:10.1039/C4RA10991K
47. Kuroda K, DeGrado WF. Amphiphilic polymethacrylate derivatives as antimicrobial agents. *J Am Chem Soc*. 2005;127:4128–4129.
48. Bougnoux ME, Aanensen DM, Morand S, Théraud M, Spratt BG, d'Enfert C. Multilocus sequence typing of candida albicans: strategies, data exchange and applications. *Infect Genet Evol*. 2004;4:243–252. doi:10.1016/j.meegid.2004.06.002
49. Zhang Y, Zhong SL, Zhang MS, Lin YC. Antibacterial activity of silver-loaded zeolite A prepared by a fast microwave-loading method. *J Mater Sci*. 2009;44:457–462. doi:10.1007/s10853-008-3129-5
50. Gao BJ, Lv YX, Jiu HF. Synthesis and properties of cationic polyacrylamide containing pyridine quaternary salt. *Polym Int*. 2003;52:1468–1473. doi:10.1002/pi.1248
51. Zachariadis PC, Hadjikakou SK, Hadjiliadis N, et al. Synthesis, Characterization and in vitro study of the cytostatic and antiviral activity of new polymeric silver(I) complexes with ribbon structures derived from the conjugated heterocyclic thioamide 2-mercapto-3,4,5,6-tetrahydropyrimidine. *Eur J Inorg Chem*. 2004;2004:1420–1426. doi:10.1002/ejic.200300672
52. Williams DW, Kuriyama T, Silva S, Malic S, Lewis MA. Candida biofilms and oral candidosis: treatment and prevention. *Periodontol*. 2000;2011(55):250–265.